

Barred galaxies in the EAGLE cosmological hydrodynamical simulation

David G. Algorry,^{1,2★} Julio F. Navarro,^{3,4} Mario G. Abadi,^{1,2} Laura V. Sales,⁵
Richard G. Bower,⁶ Robert A. Crain,⁷ Claudio Dalla Vecchia,^{8,9} Carlos S. Frenk,⁶
Matthieu Schaller,⁶ Joop Schaye¹⁰ and Tom Theuns⁶

¹*Instituto de Astronomía Teórica y Experimental, CONICET-UNC, Laprida 854, X5000BGR, Córdoba, Argentina*

²*Observatorio Astronómico de Córdoba, Universidad Nacional de Córdoba, Laprida 854, X5000BGR, Córdoba, Argentina*

³*Department of Physics & Astronomy, University of Victoria, Victoria, BC V8P 5C2, Canada*

⁴*Senior CIFAR Fellow*

⁵*Department of Physics and Astronomy, University of California, Riverside, CA 92521, USA*

⁶*Institute for Computational Cosmology, Department of Physics, Durham University, South Road, Durham, DH1 3LE, UK*

⁷*Astrophysics Research Institute, Liverpool John Moores University, 146 Brownlow Hill, Liverpool L3 5RF, UK*

⁸*Instituto de Astrofísica de Canarias C/ Vía Láctea s/n 38205 La Laguna, Tenerife, Spain*

⁹*Departamento de Astrofísica, Universidad de La Laguna, Av. del Astrofísico Francisco Sánchez s/n, 38206 La Laguna, Tenerife, Spain*

¹⁰*Leiden Observatory, Leiden University, PO Box 9513, 2300 RA Leiden, the Netherlands*

Accepted 2017 April 25. Received 2017 April 21; in original form 2016 September 16

ABSTRACT

We examine the properties of barred disc galaxies in a Λ CDM cosmological hydrodynamical simulation from the EAGLE project. Our study follows the formation of 269 discs identified at $z = 0$ in the stellar mass range $10.6 < \log M_*/M_\odot < 11$. These discs show a wide range of bar strengths, from unbarred discs (≈ 60 per cent) to weak bars (≈ 20 per cent) and to strongly barred systems (≈ 20 per cent). Bars in these systems develop after redshift ≈ 1.3 , on time-scales that depend sensitively on the strength of the pattern. Strong bars develop relatively quickly (in a few Gyr, or roughly ~ 10 disc rotation periods) in systems that are disc dominated, gas poor, and have declining rotation curves. Weak bars develop more slowly in systems where the disc is less gravitationally important, and are still growing at $z = 0$. Unbarred galaxies are comparatively gas-rich discs whose rotation speeds do not exceed the maximum circular velocity of the haloes they inhabit. Bar lengths compare favourably with observations, ranging from 0.2 to 0.8 times the radius containing 90 per cent of the stars. Bars slow down remarkably quickly as they grow, causing the inner regions of the surrounding dark halo to expand. At $z = 0$ strong bars in simulated galaxies have corotation radii roughly 10 times the bar length. Such slow bars are inconsistent with the few cases where pattern speeds have been measured or inferred observationally, a discrepancy that, if confirmed, might prove a challenge for disc galaxy formation in Λ CDM.

Key words: Galaxy: disc – Galaxy: formation – Galaxy: structure – Galaxies: kinematics and dynamics.

1 INTRODUCTION

The stellar discs of spiral galaxies are dynamically fragile structures prone to morphological and dynamical transformation. These might be triggered by external processes, such as accretion events, mergers or the tidal effects of satellites and neighbouring galaxies. They may also result from internal processes, which tend to be more subtle and to operate over longer time-scales, but are none the less effective at inducing notable changes in the morphology and

structure of the disc. Internal processes invariably redistribute the disc's angular momentum, driving mass inwards while pushing angular momentum outwards.

Angular momentum redistribution requires non-axisymmetric features (Lynden-Bell & Kalnajs 1972; Tremaine & Weinberg 1984), of which bars – i.e. extended and radially coherent $m = 2$ perturbations to the disc's azimuthal structure – are a particularly clear example. Bars come in many different sizes and shapes: from short inner bars that affect a small fraction of stars to long bars that extend out to the confines of the disc and from fat oval structures that correspond to a single dominant $m = 2$ mode to thin rectangular bars with sizable contributions from higher order even Fourier

* E-mail: david@oac.unc.edu.ar

modes. Taking them all together, bars are an extremely common phenomenon in disc galaxies, and are present in a large fraction of discs (e.g. Eskridge et al. 2000; Whyte et al. 2002; Marinova & Jogee 2007; Menéndez-Delmestre et al. 2007; Sheth et al. 2008; Gadotti 2011).

The origin of bars has long been an issue of debate. N -body discs quickly turned into bars in early simulations (Miller & Prendergast 1968; Hockney & Hohl 1969), a result that suggested a ‘global instability’ that would affect essentially all stellar discs unless stabilized by a suitable mechanism (see Sellwood & Wilkinson 1993, for a review of early work). One such mechanism was proposed by Ostriker & Peebles (1973), who argued, in an influential paper, that cold stellar discs required the presence of a massive non-rotating dark halo in order not to go bar unstable. In this scenario, bars develop quickly in systems where the disc is dominant (perhaps triggered by accretion events or tides), whereas unbarred discs are those whose dynamics is largely dominated by the dark halo (Efstathiou, Lake & Negroponte 1982). This idea is still widely in use and criteria for instantaneous ‘bar instability’ are a key ingredient of semi-analytic models of galaxy formation that attempt to match the morphological mix of the observed galaxy population (see e.g. Lacey et al. 2016, and references therein).

More recent work, however, has led to a more nuanced view, and it is now recognized that bars, weak and strong, may develop gradually in most stellar discs that are relatively massive and kinematically cold, even when the halo is important. Indeed, in some cases massive haloes have even been found to promote bar formation: one clear example is that provided by Athanassoula (2002), who shows that bars may develop faster in disc-dominated systems, but they eventually become stronger in halo-dominated ones. Haloes apparently do not prevent bars, but, rather, just delay their formation (see Athanassoula 2013, for a recent review).

Once formed, bars are a conduit for the transfer of angular momentum from the disc to other parts of the system. The more angular momentum a bar is able to lose, the longer and thinner (‘stronger’) it can become. To grow, then, bars need material to absorb the angular momentum lost by stars that join the bar, be it other stars in the outer disc or particles in the halo that might get trapped in resonances with the bar. A massive halo can therefore aid this process by providing a sink for the angular momentum lost by stars that make up the growing bar (Athanassoula 2003).

Bars can therefore develop gradually over many orbital periods, on a time-scale that depends mainly on the relative importance of disc versus halo, but likely influenced as well by the velocity dispersion of the disc (hotter discs are less prone to global distortions) and by the potential well depth of the halo (faster moving halo particles are harder to trap into resonances with the bar). The two scenarios – instantaneous bar instability versus gradual bar growth – should in principle yield different predictions for the abundance, size and pattern speeds of bars, as well as for their evolution with redshift, but detailed predictions in a proper cosmological setting have yet to be worked out.

One corollary of gradual bar formation is that bars that grow longer/stronger should slow down (Hernquist & Weinberg 1992; Debattista & Sellwood 2000). This is because bars cannot extend beyond corotation, the radius where the angular speed of a circular orbit equals that of the bar pattern (Contopoulos 1980). Angular speeds decrease outwards, so the longer the bar grows the slower its pattern speed must become. The bar cannot grow longer than the disc, of course, but it can continue to slow down, implying that the ratio between corotation radius (r_{corot}) and bar length (l_{bar}) can provide interesting constraints on the relative importance of the

disc and halo, as well as on the time elapsed since the onset of the bar (Debattista & Sellwood 2000). Although the measurements are challenging and often indirect, most observational estimates point to ‘fast bars’ where $r_{\text{corot}} < 1.4 l_{\text{bar}}$ (see e.g. Elmegreen et al. 1996; Debattista & Sellwood 2000).

Interestingly, bar slowdown might also have discernible effects on the dark matter density profile, since it is the halo that absorbs much of the disc angular momentum, especially in the case of strong bars. A number of studies have indeed suggested that the central density cusps expected in cold dark matter haloes (Navarro, Frenk & White 1996, 1997) might be softened and perhaps erased¹ by a bar (Weinberg & Katz 2002; Holley-Bockelmann, Weinberg & Katz 2005). This result has important consequences for models of gamma-ray emission by dark matter annihilation in the direction of the Galactic Centre (Schaller et al. 2016): the Milky Way is, after all, a barred galaxy (e.g. Blitz & Spergel 1991).

The discussion above suggests that the abundance of barred galaxies, together with the distribution of bar strengths, lengths and pattern speeds, may provide interesting constraints on the mass, size and kinematics of disc galaxies, on the time of their assembly, and on the mass and density profiles of the dark matter haloes they inhabit. This is important, because, once a cosmological model has been adopted, the very same properties that govern bar growth are independently specified by other constraints, and cannot be tuned arbitrarily. Success in reproducing the properties of the barred galaxy population in a particular cosmology is thus far from assured.

In Λ CDM models – the current paradigm of structure formation – the relation between galaxy mass and halo mass may be derived using ‘abundance matching’ arguments (Frenk et al. 1988; Vale & Ostriker 2006; Guo et al. 2010; Behroozi et al. 2013; Moster, Naab & White 2013). Further, galaxy sizes are also constrained by scaling laws such as the Tully–Fisher relation (see e.g. Ferrero et al. 2017). Do galaxies that match those constraints also result in a barred galaxy population whose statistics, bar lengths and pattern speeds are compatible with observation?

We address this question here by examining the properties of disc galaxies in the EAGLE cosmological hydrodynamical simulation of a Λ CDM universe (Crain et al. 2015; Schaye et al. 2015). This paper is organized as follows. In Section 2, we briefly describe the numerical simulations and the galaxy sample selection. Section 3 presents the results of our analysis, including the frequency of bars (Section 3.2), bar lengths (Section 3.3), bar growth (Section 3.5), bar slowdown (Section 3.6), and its effects on the halo mass profile (Section 3.7). We summarize our main conclusions in Section 4.

2 NUMERICAL SIMULATION AND SAMPLE SELECTION

2.1 The EAGLE simulation

We use galaxies identified in one of the cosmological hydrodynamical simulations of the EAGLE (Evolution and Assembly of GaLaxies and their Environments) Project. This run, labelled ‘Ref-L100N1504’ in Schaye et al. (2015), follows the evolution of 2×1504^3 particles (baryons + dark matter) in a large cosmological box 100 comoving Mpc on a side, adopting a flat Λ CDM cosmology consistent with the cosmological parameters from the

¹ Others, however, have argued otherwise, so the issue is still under debate (Sellwood 2003, 2008; Dubinski, Berentzen & Shlosman 2009).

Planck Collaboration XXIX (2016): $H_0 = 67.77 \text{ km s}^{-1}$, $\sigma_8 = 0.8288$, $n_s = 0.9611$, $\Omega_m = 0.307$, $\Omega_\Lambda = 0.693$ and $\Omega_b = 0.04825$.

Initial conditions were generated using second-order Lagrangian perturbation theory (Jenkins 2010) for gas and dark matter particles with masses equal to 1.81×10^6 and $9.70 \times 10^6 M_\odot$, respectively. The Plummer-equivalent gravitational softening was fixed at 2.66 kpc in comoving units until redshift $z = 2.8$ and at $2.66/(1 + 2.8) = 0.7$ kpc in physical units thereafter. Full particle properties were recorded at 29 snapshots between redshift 20 and 0. In addition, a reduced set of particle properties is recorded at 405 outputs between redshift 20 and 0. For a detailed description of the simulations, we refer the reader to Schaye et al. (2015).

The simulation was performed using a modified version of the GADGET3 code, a descendant of GADGET2 (Springel 2005), with a version of Smoothed Particle Hydrodynamics (SPH) technique modified to a pressure-entropy formulation of the equations of motion (Hopkins 2013; Schaller et al. 2015b). The simulation includes a prescription for radiative cooling and heating implemented following Wiersma, Schaye & Smith (2009).

Star formation is treated stochastically following the pressure-dependent Kennicutt–Schmidt relation (Schaye & Dalla Vecchia 2008), with a metal-dependent density threshold (Schaye 2004). The stellar initial mass function is assumed to be that of Chabrier (2003) and the stellar mass loss is modelled as in Wiersma, Schaye & Smith (2009). Feedback from star formation is implemented thermally and stochastically following Dalla Vecchia & Schaye (2012). Black holes growth is modelled using a modified version of the Bondi–Hoyle accretion and can input energy to their surrounding gas through AGN feedback (Rosas-Guevara et al. 2016).

The subgrid parameters of EAGLE have been calibrated to match the galaxy stellar mass function and the average size of galaxies as a function of mass at $z \sim 0$. Earlier papers have demonstrated that EAGLE broadly reproduces a number of well-known properties of the galaxy population, including their colours, metallicities, alpha-enhancement, star formation rates, gas content and scaling laws (Furlong et al. 2015; Lagos et al. 2015; Rahmati et al. 2015; Schaller et al. 2015a; Schaye et al. 2015; Trayford et al. 2015, 2016; Bahé et al. 2016; Camps et al. 2016; Segers et al. 2016).

2.2 Galaxy sample

Dark matter haloes are identified at every snapshot using a friends-of-friends (FoF) algorithm with linking length equal to 0.2 times the mean interparticle separation (Davis et al. 1985). Baryonic particles are then assigned to the same FoF halo as their closest dark matter neighbour. Gravitationally bound subhaloes are then identified in each FoF halo using the SUBFIND algorithm (Springel, Yoshida & White 2001; Dolag et al. 2009). We shall consider only the most massive (‘central’) subhalo of each FoF grouping and neglect ‘satellite’ galaxies in the analysis that follows.

Our sample selects systems in a narrow range of stellar mass, $10.6 \leq \log(M_*/M_\odot) \leq 11$, measured within a sphere of 30 kpc radius centred at the potential minimum of the halo. We shall refer to the radius containing half of all stars as r_{50} and that containing 90 per cent of all stars as r_{90} .

We focus our analysis on individual galaxies resolved with at least 20 000 star particles and more than 100 000 dark matter particles, so as to be able to discern their morphological traits (discs, spheroids, bars) and measure their internal structure. This resolution is at the limit of what is currently achievable in simulations that aim to resolve the galaxy population in a cosmologically significant volume. Although it is by no means ideal to follow in

detail the intricate internal dynamics governing the evolution of barred galaxies (many authors argue that many millions of particles per galaxy are required; see e.g. Weinberg & Katz 2007a), we believe that this is still an instructive exercise, especially because ours is one of the first studies of barred galaxies *as a population* in a proper cosmological setting. Earlier work has mainly focused on ‘zoom-in’ simulations of individual systems (Curir, Mazzei & Murante 2006; Kraljic, Bournaud & Martig 2012; Scannapieco & Athanassoula 2012; Guedes et al. 2013; Okamoto, Isoe & Habe 2015; Goz et al. 2015) and therefore cannot address the questions we pose here.

There are 495 central galaxies that satisfy our selection criteria at $z = 0$. Fig. 1 shows some of the properties of this sample. As a function of stellar mass, the left panel shows the virial² mass of the system and the middle panel shows its flattening, using the axis ratio c/a of the (normalized) inertia tensor principal axes, whereas the right-hand panel shows the vertical (i.e. along the axis parallel to the stars’ angular momentum) velocity dispersion, σ_z , in units of the total velocity dispersion of stars in the system, σ_{tot} .

As shown by the solid line in the left-hand panel of Fig. 1, EAGLE central galaxies in this mass range follow roughly the abundance-matching relation expected between M_* and M_{200} from the model of Guo et al. (2010). We identify discs as flattened systems kinematically cold in the vertical direction that satisfy simultaneously the following two conditions: $c/a < 0.63$ and $\sigma_z < 0.5 \sigma_{\text{tot}}$, where $\sigma_z^2 = \Sigma(v_z - \langle v_z \rangle)^2/N$ is the vertical velocity dispersion, N is the number of stellar particles and σ_{tot} is the total 3D velocity dispersion defined by $\sigma_{\text{tot}}^2 = \sigma_x^2 + \sigma_y^2 + \sigma_z^2$.

Discs are shown as coloured filled circles in Fig. 1; other galaxies are shown as either open triangles (‘spheroidals’) or crosses for ongoing mergers identified through individual visual inspection. Our final sample contains 269 discs, 193 spheroidals and 33 ongoing mergers. We shall only consider discs in the analysis that follows. We divide the sample of discs into three categories: different hues of red for strong bars, of green for weak bars and of blue for unbarred systems (Section 3.1). Note that strong bars tend to be located in thicker discs with higher vertical velocity dispersion (right-hand panel of Fig. 1). This result is somewhat obscured in the distribution of axis ratios c/a (middle panel) because, at fixed disc aspect ratio, bars have systematically lower values of c/a than azimuthally symmetric discs.

3 RESULTS

3.1 Bars in simulated discs

We identify bars in our simulated discs by measuring the amplitude of the $m = 0$ and $m = 2$ Fourier modes of the azimuthal distribution of disc particles in the plane perpendicular to the angular momentum vector of stars in the galaxy. In practice, we measure

$$a_m(R) = \sum_{i=1}^{N_R} M_i \cos(m \phi_i) \quad (1)$$

and

$$b_m(R) = \sum_{i=1}^{N_R} M_i \sin(m \phi_i), \quad (2)$$

² Throughout this paper, virial quantities are computed within radius where the enclosed density is 200 times the critical density of the Universe and are denoted by a ‘200’ subscript.

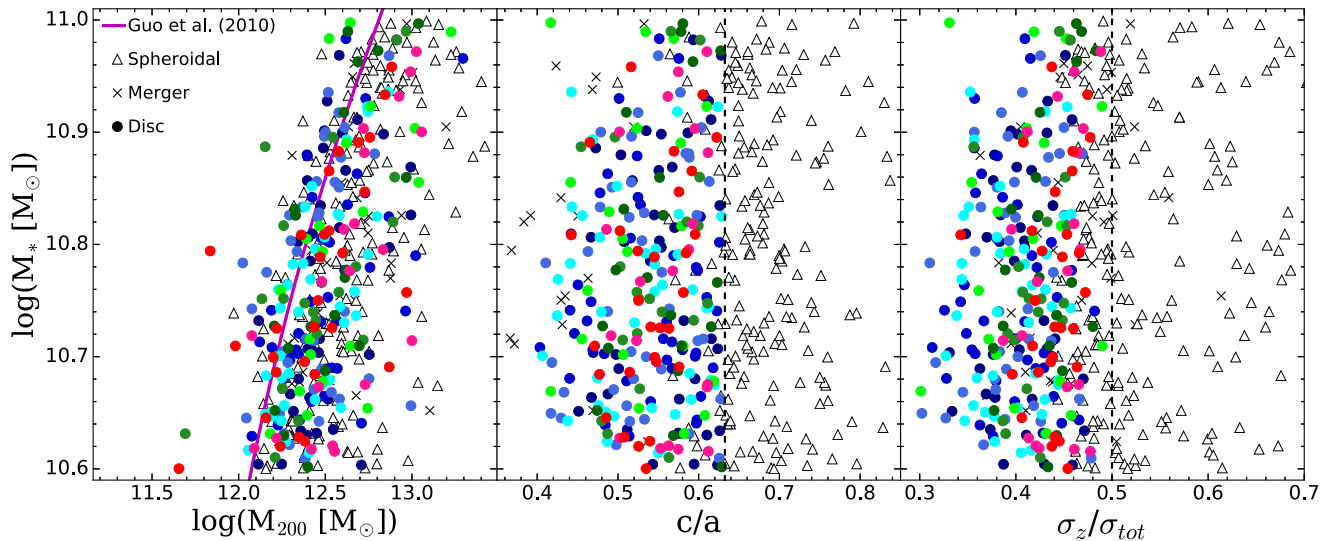


Figure 1. Disc galaxy sample from EAGLE used in this paper. *Left:* Galaxy stellar mass, M_* , as a function virial mass M_{200} . Solid line indicates the prediction of the abundance-matching model of Guo et al. (2010), for reference. *Middle:* Stellar flattening parameter c/a , measured as the ratio of the eigenvalues of the principal axes of the inertia tensor of the stars. *Right:* Minor axis stellar velocity dispersion, expressed in units of the total. Vertical dashed lines indicate the conditions required to be selected as ‘discs’ in our analysis. Discs are shown as coloured circles, spheroidal systems as open triangles and visually identified ongoing mergers or disturbed systems as crosses. The colour scheme denotes the strength of the bar pattern (see Fig. 3).

where N_R is the number of stellar particles in a given cylindrical annulus of mean radius R , M_i is the mass of the i -th particle and ϕ_i is its azimuthal angle (Athanasoula 2012).

We use the ratio

$$A_2(R) = \frac{\sqrt{a_2^2 + b_2^2}}{a_0} \quad (3)$$

to measure the strength of the $m = 2$ mode, and shall use its maximum value $A_2^{\max} = \max(A_2(R))$ as a measure of the strength of the bar component.

Fig. 2 shows projected stellar density maps for three simulated galaxies with different values of A_2^{\max} . The top row shows a galaxy with $A_2^{\max} \approx 0.1$, where no obvious bar is present (Galaxy 1). The middle row shows a system with a clear oval structure resembling a weak bar (Galaxy 2; $A_2^{\max} \approx 0.35$). Finally, the bottom row shows a strongly barred case, where $A_2^{\max} \approx 0.6$ (Galaxy 3). We shall hereafter use the value of A_2^{\max} to classify galaxies as unbarred ($A_2^{\max} < 0.2$), weakly barred ($0.2 < A_2^{\max} < 0.4$) and strongly barred ($A_2^{\max} > 0.4$). Although A_2^{\max} could in principle also be large for two-armed spirals, these typically peak at lower values than those we have used to define bars. We have visually checked every galaxy to make sure that our barred galaxies do not include spurious cases.

The right-hand column of Fig. 2 shows the radial profile of A_2 for the three examples, and indicates a few characteristic radii: r_{50} , r_{90} and the bar length, l_{bar} , which we define as the radius where the A_2 profile first dips below 0.15 after reaching its peak. Various circles indicate these radii on the galaxy images; note that this definition of l_{bar} (dashed circles) coincides well with the radial extent of the bar, as measured from the face-on map of the stellar distribution.

Finally, we shall use $\phi_{\text{bar}} = 0.5 \tan^{-1}(b_2/a_2)$, measured at the radius where $A_2(R)$ peaks, to define the bar position angle. The time variation of this angle is used to estimate the bar pattern speed in the analysis that follows.

3.2 Bar frequency

Although qualitatively there is broad consensus that bars are relatively common, quantitatively there is less agreement on the fraction of discs that are barred. This is a result of several factors, including the facts that (i) there is no standard definition of what constitutes a bar; (ii) bar prominence depends on wavelength (stronger in the infrared; e.g. Eskridge et al. 2000), morphological type (longer in early-type spirals; e.g. Elmegreen & Elmegreen 1985), galaxy mass (decreasing with increasing mass; e.g. Nair & Abraham 2010) and redshift (less frequent at early times; e.g. Sheth et al. 2008); and (iii) various studies differ on how to define the parent population of discs (would a galaxy be classified as barred or as a spheroid if it had no obvious disc component?).

Although these shortcomings hinder a definitive comparison of our results with observations, we contrast our findings with a few recent observational estimates in Fig. 3. This figure shows the cumulative distribution of our bar strength parameter A_2^{\max} and compares it with the bar fraction estimates of several studies that report bar fractions (with their respective error bar) as a function of galaxy mass.

More specifically, Barazza, Jogee & Marinova (2008) report a fraction of ≈ 38 per cent for galaxies in the mass range considered in our analysis. On the other hand, Sheth et al. (2008) find, at low redshift and in the same mass range, a much higher bar fraction of ≈ 62 per cent. Nair & Abraham (2010) report a much lower bar fraction of only about 30 per cent in a comparable mass range. Finally, Cervantes-Sodi et al. (2013) and Díaz-García et al. (2016) report similar bar fractions of 46 per cent and 45 per cent, respectively, in the corresponding mass range. Given these disparate estimates, our finding that about 40 per cent of EAGLE discs have bars (weak or strong) seems reasonably consistent with observational results.

3.3 Bar lengths

As discussed in Section 1, the length of a bar is an important parameter characterizing the evolutionary stage of the bar phenomenon.

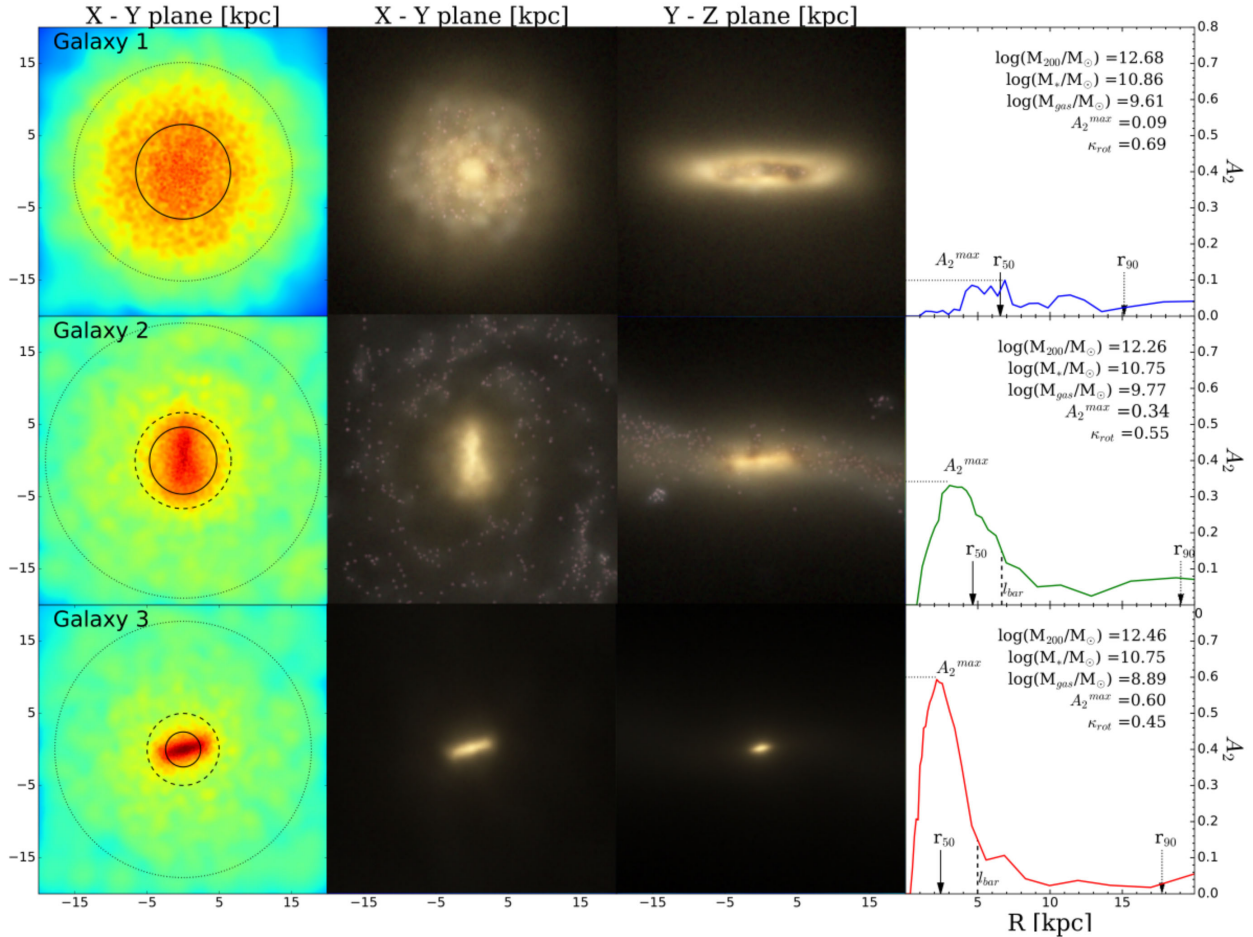


Figure 2. Projected stellar density maps for three examples of an unbarred galaxy (top row), a weak bar (middle row) and a strongly barred disc (bottom row). The leftmost column shows face-on views of the three galaxies. Dotted, dashed and solid circles on the images indicate the galaxy radius, r_{90} , the bar length, l_{bar} , and the stellar half-mass radius, r_{50} . The middle and right-hand panels show face-on and edge-on views, respectively, created with the radiative transfer code SKIRT (Baes, Dejonghe & Davies 2011). These images show the stellar light based on monochromatic SDSS u -, g - and r -band filters and accounting for dust extinction. The rightmost column shows the radial profile of the bar strength parameter, $A_2(R)$, and indicates a few characteristic radii.

Bars are expected to grow longer with time so, if bars were triggered too early and/or their growth time-scales were too short, then bar lengths, when expressed in units of the disc characteristic radii, would be too long. Such concerns have been raised by Erwin (2005), for example, who argue that there is a shortage of ‘short bars’ in simulations.

We examine the bar length l_{bar} in Fig. 4, as a function of the 90 per cent mass radius (filled circles) of all barred (weak and strong) galaxies of our sample. We also show, with crosses, observational results for the SDSS barred galaxy sample of Gadotti (2011) in the same mass range we used. Bar lengths span the whole available range: the shortest bars have $l_{\text{bar}} \sim 0.15 r_{90}$; the longest reach $l_{\text{bar}} = r_{90}$ and even exceed it in a few cases.

At comparable stellar mass, EAGLE bars show similar sizes but are hosted in larger discs. We conclude that bar lengths in EAGLE galaxies are well within the range allowed by observations, and that there is no shortage of short bars in our simulations, at least as measured by l_{bar}/r_{90} .

3.4 Barred galaxy properties at $z = 0$

We now explore the relation (at $z = 0$) between bar strength and the properties of the discs in which they form. Fig. 5 shows that

bars are stronger in discs that are more centrally concentrated (i.e. smaller half-mass radii), that bars are relatively gas poor, and that they have formed fewer stars in the past Gyr than other discs.

Indeed, unbarred galaxies in our sample are typically forming stars at rates roughly about 40 per cent of their past average. However, star formation rates decrease strongly with increasing bar strength, to roughly 1 per cent of the past average for the strongest bars. A related result is that barred discs differ strongly from unbarred ones in their star formation history. Indeed, on average, 50 per cent (90 per cent) of all stars in our strong bars have formed by cosmic time $t = 3.76$ (6.15) Gyr, compared with $t = 5.45$ (11.06) Gyr for unbarred systems.

It is intriguing that, at least for strong bars, the formation of the bar coincides with a precipitous decline in the star formation activity of the galaxy. This might be due to the fact that the bar may channel gas to the centre of the galaxy, where it would be quickly consumed, or, alternatively, to the fact that bars are more compact, denser systems where gas consumption time-scales are shorter. We do note that observed bars in general are not forming stars profusely (Barazza et al. 2008; Aguerri, Méndez-Abreu & Corsini 2009), with additional dependence on galaxy colour and mass (Masters et al. 2011; Cervantes-Sodi et al. 2013; Vera, Alonso & Coldwell 2016). Unfortunately, the limited numerical resolution of our simulations

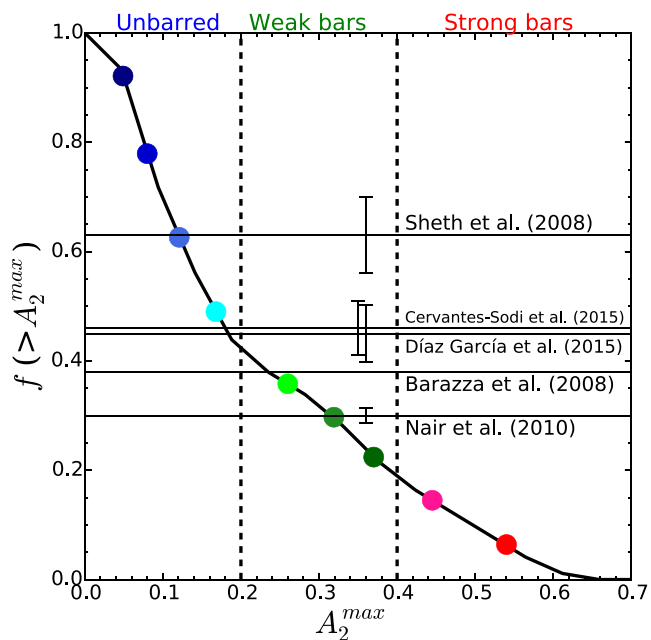


Figure 3. Cumulative distribution of the bar strength parameter A_2^{\max} , compared with observational estimates of the bar fraction of galaxies with comparable stellar mass. Error bars are shown for each observational estimate. The colour scheme assigns different hues of red to strong bars ($A_2^{\max} > 0.4$), of green to weak bars ($0.2 < A_2^{\max} < 0.4$), and of blue to unbarred systems ($A_2^{\max} < 0.2$).

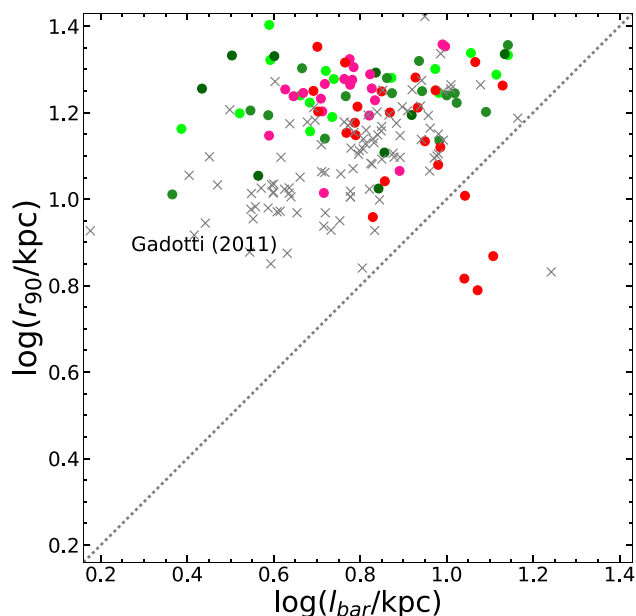


Figure 4. Bar length compared with the radius that contains 90 per cent of the stellar mass for galaxies with $A_2^{\max} > 0.2$. Colours indicate bar strength, as in Fig. 3. Grey crosses indicate results from the SDSS observations of Gadotti (2011) in the same mass range of our sample.

prevents us from providing a more conclusive answer to this question.

As shown by Fig. 5, strongly barred discs are roughly three times smaller than unbarred systems of similar stellar mass. This is an important clue that bar formation proceeds more rapidly in systems where the stellar component is more gravitationally

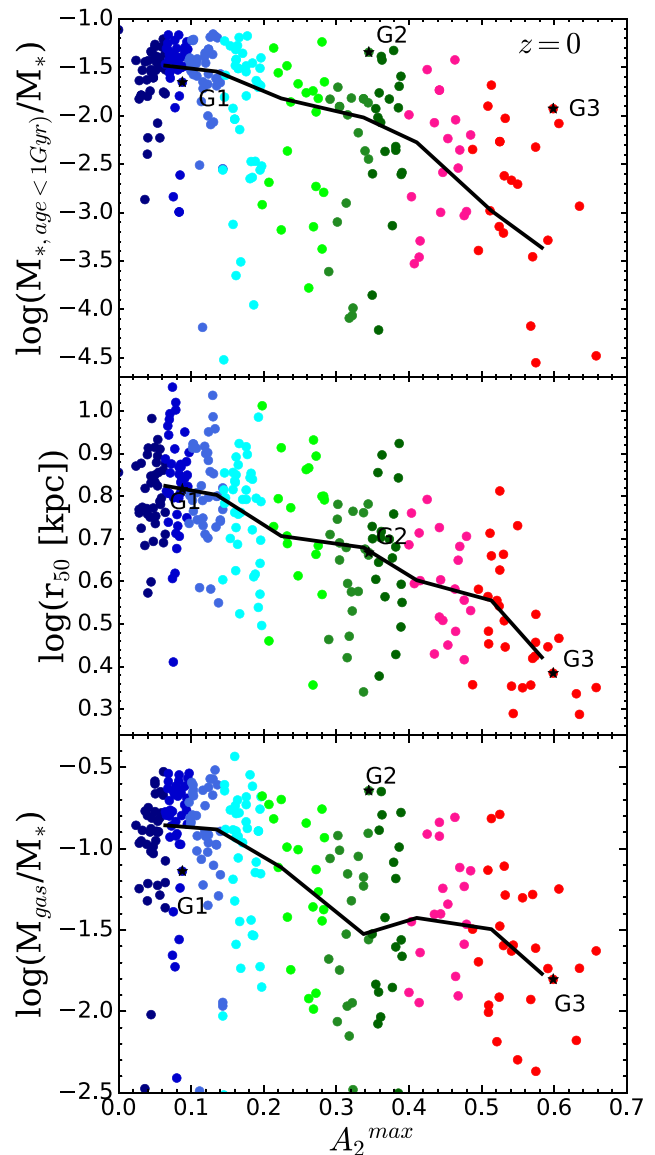


Figure 5. Bar strength parameter A_2^{\max} as a function of gas mass fraction (bottom), of half-mass radius (middle) and of the stellar mass form in the last Gyr at $z = 0$ for all discs in our sample. Solid lines trace the median as a function of bar strength. G1, G2 and G3 refer to galaxies 1, 2 and 3 in Fig. 2, respectively.

dominant. We turn our attention to the time-scale of bar growth next.

3.5 Bar growth

Fig. 6 shows the evolution of the bar strength parameter, averaged for galaxies binned as a function of their value of A_2^{\max} at $z = 0$, for the sake of clarity. This shows that bars have developed in these systems only in the past 8 Gyr; indeed, at $z \sim 1.3$ ($t \sim 5$ Gyr) very few, if any, of the present-day EAGLE discs in our sample had a measurable bar. Note that this statement applies only to the current sample, and should *not* be understood as implying that the bar fraction in EAGLE necessarily declines with redshift. We intend to address that topic in future work, but restrict ourselves here to the evolution of $z = 0$ EAGLE discs within a narrow range of stellar mass, as described in Section 2.2.

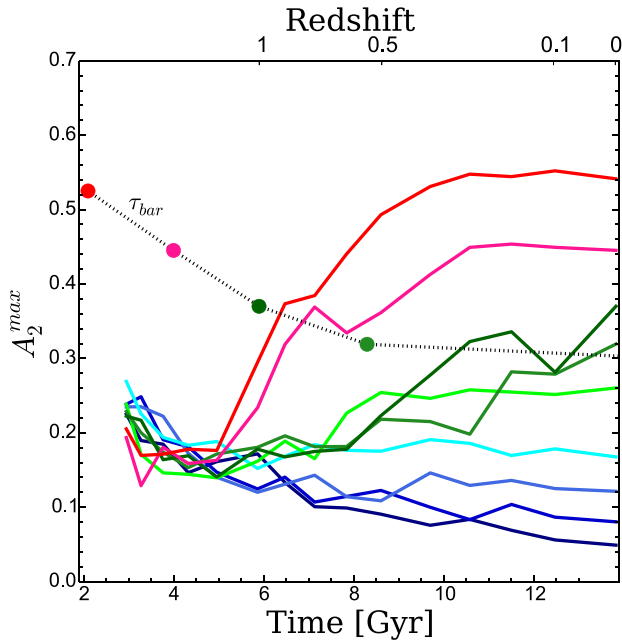


Figure 6. Evolution of the bar strength parameter, averaged in bins of galaxies according to their value of A_2^{\max} at $z = 0$. Colour scheme for the curves is as in Fig. 3. Bar growth time-scales (defined arbitrarily as the time it takes to increase the bar strength from 0.2 to 0.4) are shown by the grey connected symbols. Note that this approaches the Hubble time for the weakest bars.

Fig. 6 illustrates a number of interesting points: (i) bars, especially strong ones, are in general not a recurrent phenomenon; (ii) strong bars develop quickly and saturate, whereas weak bars are still growing at $z = 0$; (iii) few unbarred galaxies have had bars in the past; and, finally, (iv) the time-scale for bar growth is clearly a strong function of final bar strength. (We have explicitly checked that none of these conclusions are a result of the averaging procedure.) We illustrate this by the dotted line in Fig. 6, which indicates the time-scale τ_{bar} (defined as the time needed for a bar to grow from $A_2^{\max} = 0.2$ to 0.4) as a function of final bar strength.

Note that even strong bars grow over several Gyr, or tens of half-mass disc rotation periods.³ Weak bars take much longer to develop. We conclude that bars in EAGLE discs are best described as developing gradually over many rotation periods rather than as the result of a ‘global instability’ that proceeds nearly instantaneously when triggered.

What sets the bar growth time-scale? Or, more generally, what parameter best predicts the development of a bar? A clue may be gleaned from Fig. 5, where we showed that barred discs are on average more centrally concentrated than unbarred ones: this is in agreement with the findings of earlier work which suggested that gravitationally dominant discs are the ones where bars will grow faster (see Section 1). A simple quantitative estimate is given by the ratio between the circular velocity at the half-mass radius, $V_{50} = V_c(r_{50})$, and the disc contribution, $V_{\text{disc}} = (GM_*/r_{50})^{1/2}$,

$$f_{\text{disc}} \equiv \frac{V_{50}}{V_{\text{disc}}}. \quad (4)$$

³ The average disc rotation period of discs in our sample at $r = 5$ kpc is 0.14 Gyr.

This type of formulation was first proposed by Efstathiou et al. (1982) and is the one usually adopted in semi-analytic models such as GALFORM (see e.g. Cole et al. 2000; Bower et al. 2006; Lacey et al. 2016). These models typically assume that bars develop in discs with $f_{\text{disc}} < 1.1$, and that others remain unbarred.

The f_{disc} parameter measures the *local* importance of the disc but there is evidence to suggest that, on its own, it is insufficient to predict which galaxies will become barred. As discussed by Athanassoula & Misiriotis (2002) and Athanassoula (2003), simulations show not only that some ‘ f_{disc} -stable’ discs may become barred, but also that presumably unstable, low- f_{disc} systems may be stabilized when placed within massive haloes of high-velocity dispersion. In other words, what matters is not just the *local* gravitational importance of the disc, but also its *global* importance to the whole system, including its halo.

A crude measure of the latter is provided by the ratio between the circular velocity at the half-mass radius, V_{50} , and the maximum circular velocity of the surrounding halo (which typically peaks far outside the disc),

$$f_{\text{dec}} = \frac{V_{50}}{V_{\text{max,halo}}}. \quad (5)$$

With this definition, systems with $f_{\text{dec}} < 1$ are those whose circular velocity curves rise beyond the outer confines of the disc. The smaller f_{dec} the higher the velocities of halo particles are relative to the disc, which may prevent them from coupling effectively to the bar, delaying its onset or averting it altogether. Systems with $f_{\text{dec}} > 1$, on the other hand, are those with ‘declining’ rotation curves, where the disc is dominant and its rotation speed is higher than the speed of most halo particles.

We examine this in Fig. 7, where we show f_{disc} versus f_{dec} for all galaxies in our sample, measured just *before*⁴ the bar develops, at $t = t_{\text{bar}}$. This figure shows clearly that the $f_{\text{disc}} < 1.1$ criterion does not accurately predict which galaxies will become barred: 45 per cent of discs satisfying this criterion remain unbarred, and most such discs (73 per cent, to be more precise) have ‘rising’ circular velocity curves, i.e. $f_{\text{dec}} < 1$.

Fig. 7 thus suggests that combining both f_{disc} and f_{dec} improves matters. For example, the combined criteria $f_{\text{disc}} < 1$ and $f_{\text{dec}} > 0.95$ identify 82 per cent of strong bars. Of galaxies satisfying these criteria, only 11 per cent remain unbarred.

Similarly, the criteria $f_{\text{disc}} > 0.95$ and $f_{\text{dec}} < 1$ single out 77 per cent of all discs that remain unbarred. Of these, very few have developed strong bars (only 10) and 28 out of a total of 59 have developed weak bars. The latter are, perhaps unsurprisingly, much harder to predict on the basis of f_{disc} and f_{dec} alone, and are seen to span nearly the full range of allowed values in Fig. 7.

We conclude that, in order to develop strong bars, discs must be locally and globally dominant; in other words, they must contribute a large fraction of the inner mass budget to systems where the disc circular speed exceeds that of its halo. On the other hand, galaxies that remain unbarred are predominantly those where the disc is less important, not only within their half-mass radii but also in relation to their surrounding haloes.

3.6 Bar slowdown

As discussed in Section 1, we expect bars that grow gradually to slow down as they become stronger. This is indeed the case in our

⁴ In practice, we choose t_{bar} as the time when A_2^{\max} first exceeds 0.2. We set $t_{\text{bar}} = 8.6$ Gyr ($z = 0.5$) for unbarred systems.

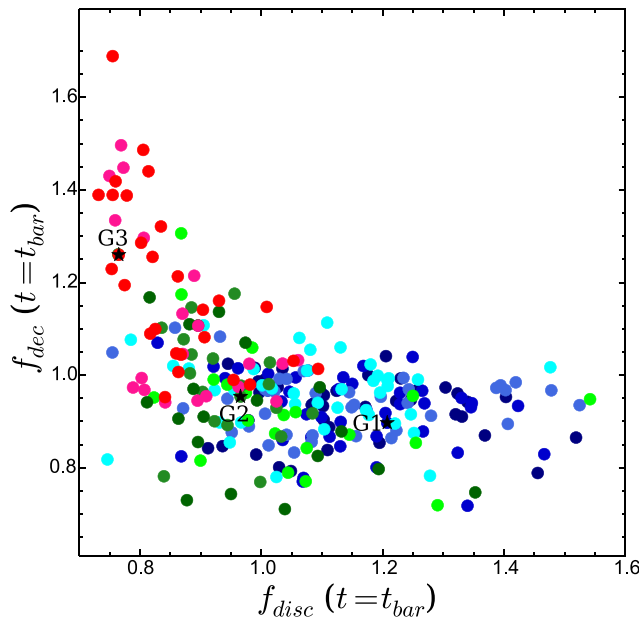


Figure 7. Disc gravitational importance at $t = t_{\text{bar}}$, defined as the time just before bars form (for weak and strong bars) or at $z = 0.5$ for unbarred discs. The parameter f_{disc} measures the contribution of the disc to the circular velocity at the half-mass radius (equation 4). The parameter f_{dec} measures the global importance of the disc to the system (equation 5). Colour scheme is as in Fig. 3. Combining f_{dec} with f_{disc} improves predictions of which discs will develop bars. See the text for definitions and further discussion.

simulations, as shown in Fig. 8. This figure shows the decline in the bar pattern speed, Ω_{bar} , since $z = 0.5$ as a function of bar length. We only show this for the ‘strong’ bars in our sample because of difficulties estimating the pattern speed of weak bars accurately.

Fig. 8 shows that Ω_{bar} has decreased on average by a factor of 3 over the past 5 Gyr. In the same time interval bar lengths have increased by a factor of 1.7 on average. Indeed, the slowdown seems to roughly satisfy the $l_{\text{bar}} \times \Omega_{\text{bar}} = \text{constant}$ relation (grey dotted line) expected for bar lengths that increase in proportion to the corotation radius in a galaxy with a flat circular velocity profile.

At late times, the slowdown proceeds in most galaxies without the corresponding increase in bar length, so that bar lengths become smaller than their corotation radii at $z = 0$. We examine this in more detail in Fig. 9, where we show r_{corot} versus l_{bar} for all strongly barred galaxies (as identified at $z = 0$) at three different redshifts ($z = 0.5$, $z = 0.27$ and $z = 0$) and compare them with the compilation of Corsini (2011) and Aguerri et al. (2015), which include only galaxies in the local universe.

Bars below the dotted line that delineates $r_{\text{corot}} = 1.4 l_{\text{bar}}$ are usually referred to as ‘fast bars’, a characterization that describes well the few galaxies for which pattern speeds have been reliably measured observationally. Note that EAGLE strong bars, although relatively fast at early times according to this characterization, have clearly become slow⁵ by $z = 0$.

Bar slowdown was first studied by Weinberg (1985), using analytic arguments and later examined in N -body numerical simulations

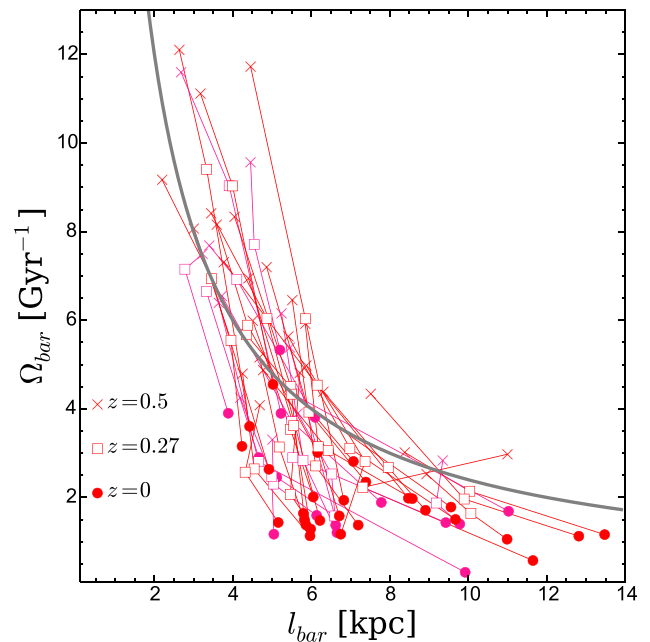


Figure 8. Pattern speed versus bar length for strong bars. This shows clearly that bars slow down as they grow. At early times this follows roughly the $l_{\text{bar}} \propto \Omega_{\text{bar}}^{-1}$ scaling expected for corotation radii in discs with flat rotation curves (grey dotted curve). At late times the pattern speed slows down with little further increase in bar length, pushing corotation well beyond the edge of the bar.

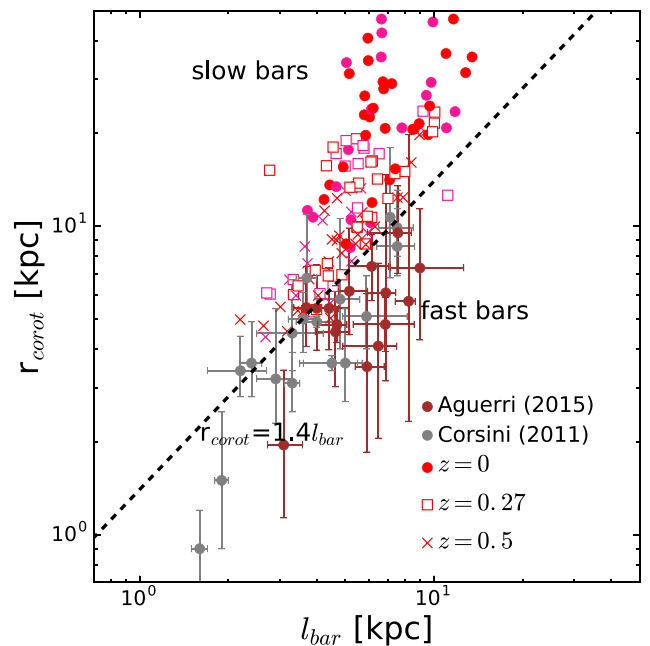


Figure 9. Corotation radius versus bar length for *strong* bars in our sample, at three different times: $z = 0.5$ (crosses), $z = 0.27$ (squares) and $z = 0$ (circles). Grey and brown symbols with error bars are observational data from the compilation of Corsini (2011) and Aguerri et al. (2015). ‘Fast bars’ are those below the dotted line delineating $r_{\text{corot}} = 1.4 l_{\text{bar}}$. Most strong bars in our simulation are ‘slow’ at $z = 0$, in contrast with observational estimates.

⁵ The few weak bars we were able to measure reliable pattern speeds for at $z = 0$ are slightly faster, but still not as fast as observed. We do not include them in Fig. 9 because we were unable to measure pattern speeds for all of them.

by Little & Carlberg (1991) and Hernquist & Weinberg (1992). The understanding of this issue is important as it could help constrain the inner dark matter content of haloes (e.g. Debattista & Sellwood 1998; O’Neill & Dubinski 2003).

Indeed, Debattista & Sellwood (2000) argued that ‘fast bars’ present a severe challenge to Λ CDM models. In their argument, dynamical friction in haloes as centrally concentrated as those expected in Λ CDM would quickly slow down a bar and push its corotation radius well beyond the edge of the bar, just as seen at $z = 0$ in Fig. 9.

The Debattista & Sellwood (2000) observation ignited a spirited debate about the true slowdown rate of bars in N -body simulations that is, as far as we can tell, still unresolved (see e.g. Sellwood 2006; Weinberg & Katz 2007a,b; Sellwood 2008, and references therein). The disagreement centres on the role of dynamical friction, which is intimately linked to the width of resonances in phase space and on the minimum numerical resolution required to properly resolve them. If the pattern speed evolves quickly, the resonance ‘broadens’ and a large fraction of particles in the halo may contribute to the slowdown, a result that has led some authors to argue that the slowdown is not critically dependent on numerical resolution (e.g. Sellwood 2006, 2008). On the other hand, Weinberg & Katz (2007a) argue that several *millions* of particles would be needed to capture the resonant coupling that slows down the bar, and warn that slowdown time-scales may be severely underestimated in simulations with limited numbers of particles.

The numerical resolution of our simulations is admittedly poor by comparison, so it is unclear whether our results may help to resolve this disagreement. We therefore just note that strong bars slow down very rapidly in our simulations, creating a population of ‘slow bars’ that, apparently, have no obvious observational counterparts. If confirmed by simulations with improved numerical resolution, this may very well present a challenge to models of barred galaxy formation in a Λ CDM universe. Resolving this issue, however, may require much higher resolution simulations than achievable today for cosmologically significant volumes.

3.7 Halo evolution

The dramatic bar slowdown discussed in the previous section suggests that the bar interacts strongly with the dark matter halo. This interaction leads to substantial exchange of energy and angular momentum, leading to substantial expansion of the inner regions of the halo. We show this in Fig. 10, where we plot, for various values of the bar strength, the evolution of the enclosed dark matter mass within two different radii, $r = 2.5$ and 5 kpc. It is clear from this figure that the slowdown of the bar induces significant expansion of the inner dark matter mass profile.

Interestingly, even weak bars are able to lower the central density of dark matter significantly, implying that non-axisymmetric features in disc galaxies might be an important driver of the transformation of the inner mass profiles of their dark matter haloes. By contrast, the inner regions of haloes of disc galaxies that do not develop a bar evolve little over the past ~ 5 Gyr or so.

Finally, Fig. 10 shows that, despite the bar-induced expansion of the inner halo, barred galaxies at $z = 0$ still have more dark matter in their inner regions than their unbarred counterparts of similar stellar and virial mass. This is mainly because barred galaxies occur predominantly in dense, dominant discs that have substantially contracted the dark matter profile before the bar forms.

Indeed, galaxies that will become strong bars have, at $z \sim 0.5$, roughly twice as much dark matter within 2.5 kpc from the centre as

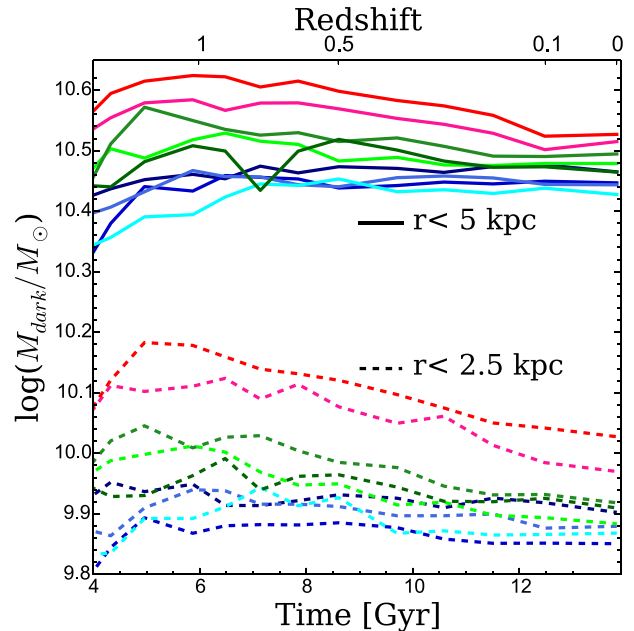


Figure 10. Evolution of the dark matter mass enclosed within two fixed physical radii, $r = 5$ kpc and $r = 2.5$ kpc, averaged for galaxies binned as a function of their bar strength at $z = 0$ (i.e. as in Fig. 6). Bar slowdown clearly reduces the central density of dark matter within the region of the bar. By contrast, the central dark matter densities of unbarred galaxies remain unchanged during the past 5–6 Gyr.

galaxies that remain unbarred. Although the difference narrows as the bar slows down, it still remains at $z = 0$. This implies that the bar-induced halo expansion might not actually create a constant density ‘core’ in a cuspy dark halo; the inner cusps of haloes of would-be bars are so steep because of contraction that even after expanding they may remain cuspy. Although qualitatively our argument seems robust, we are unable to examine it quantitatively because of limited numerical resolution: the average Power et al. (2003) convergence radius of our systems, for example, is of order ~ 5 kpc. Clarifying whether bars carve ‘cores’ out of cusps or not will need to await simulations with much higher numerical resolution.

4 SUMMARY AND CONCLUSIONS

We have used a Λ CDM cosmological hydrodynamical simulation from the EAGLE project to study the formation of barred galaxies. The simulation evolves a box 100 Mpc on a side with 2×1504^3 particles, half of which are baryonic and half dark matter. Our study focuses on a narrow range of stellar mass, $10.6 < \log M_*/M_\odot < 11$, which are resolved with at least 22 000 star particles. Of the 495 galaxies in that mass range identified at $z = 0$, we select a sample of 269 ‘discs’, defined as flattened systems with minor-to-major axis ratio $c/a < 0.63$ and relatively low vertical velocity dispersion $\sigma_z/\sigma_{\text{tot}} < 0.5$.

We identify barred galaxies by measuring the amplitude of the normalized $m = 2$ Fourier mode of the azimuthal surface density profile as a function of cylindrical radius, and choose as a measure of bar strength the peak amplitude, A_2^{max} . We consider ‘barred’ all discs with $A_2^{\text{max}} > 0.2$. We follow the evolution of all these galaxies to estimate bar growth time-scales, to identify which parameters predict the development of bars best, and to measure the evolution of bar strength, length and pattern speed.

Our main conclusions may be summarized as follows.

(i) About 40 per cent of EAGLE discs in our sample are barred, 20 per cent of them strong bars ($A_2^{\max} > 0.4$) and another 20 per cent weak bars ($0.2 < A_2^{\max} < 0.4$). This bar frequency seems in reasonable agreement with observational estimates from Barazza et al. (2008), Cervantes-Sodi et al. (2013) and Díaz-García et al. (2016).

(ii) Bars in our simulated galaxies span a wide range in terms of length, and are in reasonable agreement with observed discs of comparable stellar mass.

(iii) At $z = 0$, bar strength correlates strongly with stellar half-mass radius (stronger bars form in smaller discs), hinting that, as expected from earlier work, bars develop preferentially in systems where the disc is gravitationally important. We also find that stronger bars develop in systems that are less gas-rich, and that have formed the bulk of their stars earlier than unbarred discs.

(iv) Strong bars in our sample develop relatively quickly before saturating over a few Gyrs. Weak bars are still growing in strength at $z = 0$, and take much longer to develop, with characteristic time-scales approaching or even exceeding a Hubble time. Even our strongest, fastest growing bars take roughly 4–5 Gyr (a few dozen disc rotations) to form fully.

(v) The gravitational importance of the disc at its half-mass radius may be used to predict which galaxies will develop bars, but its predictive power may be enhanced by considering the overall importance of the disc in the system as a whole. Strong bars form in discs where baryons dominate and whose rotation speeds exceed the maximum circular velocity of the halo. Unbarred galaxies are discs where baryons are less important and whose rotation curves tend to rise in the outskirts.

(vi) Strong bars slow down quickly as they grow and, at $z = 0$ are in the ‘slow bar’ regime, $r_{\text{corot}}/l_{\text{bar}} > 1.4$. This is in contrast with the few bars whose pattern speeds have been inferred observationally, all of which are ‘fast’. This discrepancy may imply either that bar slowdown rates are artificially high in simulations at EAGLE resolution (e.g. Weinberg & Katz 2007a), or, as argued in earlier work, that producing long-lasting ‘fast bars’ is a real challenge for Λ CDM (e.g. Debattista & Sellwood 2000).

(vii) The bar slowdown induces an expansion of the inner regions of the dark matter halo, as they capture the angular momentum of the forming bar. However, bars form in massive dense discs with heavily contracted haloes, so despite the bar-induced expansion barred galaxy haloes are still more centrally concentrated than unbarred galaxies of similar stellar mass. Our numerical resolution is not enough to let us ascertain whether this expansion may lead to the formation of constant density ‘cores’ in barred galaxy haloes.

Our overall conclusion is that current Λ CDM cosmological hydrodynamical simulations of cosmologically significant volumes such as EAGLE yield a population of simulated discs with bar fractions, lengths and evolution that are in broad agreement with observational constraints. They also confirm earlier suggestions that ‘slow bars’ might pose a severe challenge to this scenario. Although bars form in the manner and frequency expected, they slow down too fast through interaction with the dark halo. Unless the Universe has a population of slow bars that has yet to be recognized, or the bar slowdown we measure is artificially enhanced by limited numerical resolution, accounting for the presence of ‘fast bars’ in strongly barred discs is a clear goal for the next generation of Λ CDM simulations of galaxy formation.

ACKNOWLEDGEMENTS

We thank the referee for a very constructive report. DA, MGA, JFN and LVS acknowledge financial support from grant PICT-1137/2012 from the Agencia Nacional de Promoción Científica y Tecnológica, Argentina. MGA acknowledges financial support of grant 203/14 of the SECYTUNC, Argentina. We are grateful to Alejandro Benítez-Llambay for the use of his Py-SPHViewer software. The research was supported in part by the European Research Council under the European Union’s Seventh Framework Programme (FP7/2007-2013)/ERC Grant agreement 278594-GasAroundGalaxies, 267291-COSMIWAY, by the Interuniversity Attraction Poles Programme initiated by the Belgian Science Policy Office (AP P7/08 CHARM) and by the Netherlands Organisation for Scientific Research (NWO), through VICI grant 639.043.409. This work used the DiRAC Data Centric system at Durham University, operated by the Institute for Computational Cosmology on behalf of the STFC DiRAC HPC Facility (www.dirac.ac.uk). This equipment was funded by BIS National E-infrastructure capital grant ST/K00042X/1, STFC capital grants ST/H008519/1 and ST/K00087X/1, STFC DiRAC Operations grant ST/K003267/1 and Durham University. DiRAC is part of the National E-Infrastructure. RAC is a Royal Society University Research Fellow. CDV acknowledges financial support from the Spanish Ministry of Economy and Competitiveness (MINECO) under the 2015 Severo Ochoa Program SEV-2015-0548 and grant AYA2014-58308. We acknowledge the useful and thorough report of an anonymous referee.

REFERENCES

- Aguerri J. A. L., Méndez-Abreu J., Corsini E. M., 2009, *A&A*, 495, 491
Aguerri J. A. L. et al., 2015, *A&A*, 576, A102
Athanasoula E., 2002, *ApJ*, 569, L83
Athanasoula E., 2003, *MNRAS*, 341, 1179
Athanasoula E., 2012, *MNRAS*, 426, L46
Athanasoula E., 2013, *Bars and Secular Evolution in Disk Galaxies: Theoretical Input*, p. 305
Athanasoula E., Misiriotis A., 2002, *MNRAS*, 330, 35
Baes M., Dejonghe H., Davies J., 2011, *SKIRT: Stellar Kinematics Including Radiative Transfer*, Astrophysics Source Code Library, record ascl:1109.003
Bahé Y. M. et al., 2016, *MNRAS*, 456, 1115
Barazza F. D., Jogee S., Marinova I., 2008, *ApJ*, 675, 1194
Behroozi P. S., Marchesini D., Wechsler R. H., Muzzin A., Papovich C., Stefanon M., 2013, *ApJ*, 777, L10
Blitz L., Spergel D. N., 1991, *ApJ*, 379, 631
Bower R. G., Benson A. J., Malbon R., Helly J. C., Frenk C. S., Baugh C. M., Cole S., Lacey C. G., 2006, *MNRAS*, p. 659
Camps P., Trayford J. W., Baes M., Theuns T., Schaller M., Schaye J., 2016, *MNRAS*, 462, 1057
Cervantes-Sodi B., Li C., Park C., Wang L., 2013, *ApJ*, 775, 19
Chabrier G., 2003, *ApJ*, 586, L133
Cole S., Lacey C. G., Baugh C. M., Frenk C. S., 2000, *MNRAS*, 319, 168
Contopoulos G., 1980, *A&A*, 81, 198
Corsini E. M., 2011, *Memorie della Societa Astronomica Italiana Supplementi*, 18, 23
Crain R. A. et al., 2015, *MNRAS*, 450, 1937
Curir A., Mazzei P., Murante G., 2006, *A&A*, 447, 453
Dalla Vecchia C., Schaye J., 2012, *MNRAS*, 426, 140
Davis M., Efstathiou G., Frenk C. S., White S. D. M., 1985, *ApJ*, 292, 371
Debattista V. P., Sellwood J. A., 1998, *ApJ*, 493, L5
Debattista V. P., Sellwood J. A., 2000, *ApJ*, 543, 704
Díaz-García S., Salo H., Laurikainen E., Herrera-Endoqui M., 2016, *A&A*, 587, A160
Dolag K., Borgani S., Murante G., Springel V., 2009, *MNRAS*, 399, 497

- Dubinski J., Berentzen I., Shlosman I., 2009, *ApJ*, 697, 293
 Efstathiou G., Lake G., Negroponte J., 1982, *MNRAS*, 199, 1069
 Elmegreen B. G., Elmegreen D. M., 1985, *ApJ*, 288, 438
 Elmegreen B. G., Elmegreen D. M., Chromey F. R., Hasselbacher D. A., Bissell B. A., 1996, *AJ*, 111, 2233
 Erwin P., 2005, *MNRAS*, 364, 283
 Eskridge P. B. et al., 2000, *AJ*, 119, 536
 Ferrero I. et al., 2017, *MNRAS*, 464, 4736
 Frenk C. S., White S. D. M., Davis M., Efstathiou G., 1988, *ApJ*, 327, 507
 Furlong M. et al., 2015, *MNRAS*, 450, 4486
 Gadotti D. A., 2011, *MNRAS*, 415, 3308
 Goz D., Monaco P., Murante G., Curir A., 2015, *MNRAS*, 447, 1774
 Guedes J., Mayer L., Carollo M., Madau P., 2013, *ApJ*, 772, 36
 Guo Q., White S., Li C., Boylan-Kolchin M., 2010, *MNRAS*, 404–1111
 Hernquist L., Weinberg M. D., 1992, *ApJ*, 400, 80
 Hockney R. W., Hohl F., 1969, *AJ*, 74, 1102
 Holley-Bockelmann K., Weinberg M., Katz N., 2005, *MNRAS*, 363, 991
 Hopkins P. F., 2013, *MNRAS*, 428, 2840
 Jenkins A., 2010, *MNRAS*, 403, 1859
 Kraljic K., Bournaud F., Martig M., 2012, *ApJ*, 757, 60
 Lacey C. G. et al., 2016, *MNRAS*, 462, 3854
 Lagos C. d. P. et al., 2015, *MNRAS*, 452, 3815
 Little B., Carlberg R. G., 1991, *MNRAS*, 251, 227
 Lynden-Bell D., Kalnajs A. J., 1972, *MNRAS*, 157, 1
 Marinova I., Joglee S., 2007, *ApJ*, 659, 1176
 Masters K. L. et al., 2011, *MNRAS*, 411, 2026
 Menéndez-Delmestre K., Sheth K., Schinnerer E., Jarrett T. H., Scoville N. Z., 2007, *ApJ*, 657, 790
 Miller R. H., Prendergast K. H., 1968, *ApJ*, 151, 699
 Moster B. P., Naab T., White S. D. M., 2013, *MNRAS*, 428, 3121
 Nair P. B., Abraham R. G., 2010, *ApJ*, 714, L260
 Navarro J. F., Frenk C. S., White S. D. M., 1996, *ApJ*, 462, 563
 Navarro J. F., Frenk C. S., White S. D. M., 1997, *ApJ*, 490, 493
 O’Neill J. K., Dubinski J., 2003, *MNRAS*, 346, 251
 Okamoto T., Isoe M., Habe A., 2015, *PASJ*, 67, 63
 Ostriker J. P., Peebles P. J. E., 1973, *ApJ*, 186, 467
 Planck Collaboration XXIX 2016, *A&A*, 586, 132
 Power C., Navarro J. F., Jenkins A., Frenk C. S., White S. D. M., Springel V., Stadel J., Quinn T., 2003, *MNRAS*, 338, 14
 Rahmati A., Schaye J., Bower R. G., Crain R. A., Furlong M., Schaller M., Theuns T., 2015, *MNRAS*, 452, 2034
 Rosas-Guevara Y., Bower R. G., Schaye J., McAlpine S., Dalla Vecchia C., Frenk C. S., Schaller M., Theuns T., 2016, *MNRAS*, 462, 190
 Scannapieco C., Athanassoula E., 2012, *MNRAS*, 425, L10
 Schaller M. et al., 2015a, *MNRAS*, 451, 1247
 Schaller M., Dalla Vecchia C., Schaye J., Bower R. G., Theuns T., Crain R. A., Furlong M., McCarthy I. G., 2015b, *MNRAS*, 454, 2277
 Schaller M. et al., 2016, *MNRAS*, 455, 4442
 Schaye J., 2004, *ApJ*, 609, 667
 Schaye J., Dalla Vecchia C., 2008, *MNRAS*, 383, 1210
 Schaye J. et al., 2015, *MNRAS*, 446, 521
 Segers M. C., Schaye J., Bower R. G., Crain R. A., Schaller M., Theuns T., 2016, *MNRAS*, 461, L102
 Sellwood J. A., 2003, *ApJ*, 587, 638
 Sellwood J. A., 2006, *ApJ*, 637, 567
 Sellwood J. A., 2008, *ApJ*, 679, 379
 Sellwood J. A., Wilkinson A., 1993, *Reports on Progress in Physics*, 56, 173
 Sheth K. et al., 2008, *ApJ*, 675, 1141
 Springel V., 2005, *MNRAS*, 364, 1105
 Springel V., Yoshida N., White S. D. M., 2001, *New Astronomy*, 6, 79
 Trayford J. W. et al., 2015, *MNRAS*, 452, 2879
 Trayford J. W., Theuns T., Bower R. G., Crain R. A., Lagos C. d. P., Schaller M., Schaye J., 2016, *MNRAS*, 460, 3925
 Tremaine S., Weinberg M. D., 1984, *ApJ*, 282, L5
 Vale A., Ostriker J. P., 2006, *MNRAS*, 371, 1173
 Vera M., Alonso S., Coldwell G., 2016, *A&A*, 595, A63
 Weinberg M. D., 1985, *MNRAS*, 213, 451
 Weinberg M. D., Katz N., 2002, *ApJ*, 580, 627
 Weinberg M. D., Katz N., 2007a, *MNRAS*, 375, 425
 Weinberg M. D., Katz N., 2007b, *MNRAS*, 375, 460
 Whyte L. F., Abraham R. G., Merrifield M. R., Eskridge P. B., Frogel J. A., Pogge R. W., 2002, *MNRAS*, 336, 1281
 Wiersma R. P. C., Schaye J., Smith B. D., 2009, *MNRAS*, 393, 99

This paper has been typeset from a $\text{\TeX}/\text{\LaTeX}$ file prepared by the author.